Monthly Notices of the ROYAL ASTRONOMICAL SOCIETY

MNRAS **535,** 2800–2811 (2024) https://doi.org/10.1093/mnras/stae2502
Advance Access publication 2024 November 7

White dwarf–black hole binary progenitors of low-redshift gamma-ray bursts

Nicole M. Lloyd-Ronning [1,2]★ Jarrett Johnson,[2,3] Phoebe Upton Sanderbeck,[2,4]† Makana Silva[1,2]† and Roseanne M. Cheng[1,5]

[1]*Computational Physics and Methods Group, Los Alamos National Lab, Los Alamos, NM 87545, USA*
[2]*Center for Theoretical Astrophysics, Los Alamos National Lab, Los Alamos, NM 87544, USA*
[3]*X Theoretical Design Division, Los Alamos National Lab, Los Alamos, NM 87544, USA*
[4]*Information Systems and Modeling Group, Los Alamos National Lab, Los Alamos, NM 87544, USA*
[5]*Department of Physics and Astronomy, University of New Mexico, Albuquerque, NM 87106, USA*

Accepted 2024 November 3. Received 2024 October 8; in original form 2024 August 22

ABSTRACT

Although there is strong evidence that many long gamma-ray bursts (LGRBs) are associated with the collapse of a massive star, tantalizing results in recent years have upended the direct association of *all* LGRBs with massive stars. In particular, kilonova signals in some LGRB light curves as well as a suggested uptick in the rate density of LGRBs at low redshifts (deviating significantly from the star formation rate) suggest that compact object mergers may be a non-negligible fraction of the LGRB population. Here, we investigate the contribution of white dwarf–black hole mergers to the LGRB population. We present evidence for the deviation of the LGRB rate density from the star formation rate at low redshifts, and provide analytic and numerical arguments for why a white dwarf–black hole merger system may be a viable progenitor to explain this deviation. We show the range of parameter space in which the durations, energetics, and rates of these systems can account for a significant subpopulation of low-redshift LGRBs.

Key words: stars: binaries: general – stars: gamma-ray bursts: general.

1 INTRODUCTION

For many decades, we have accumulated observational evidence that has led to a general cognizance of gamma-ray burst (GRB) progenitor systems. Based on the duration of their prompt gamma-ray emission, energetics, locations in their host galaxies, associated supernovae (or lack thereof), associated kilonovae, and gravitational wave signals (or lack thereof), the following paradigm has emerged: long gamma-ray bursts (LGRBs) – GRBs with prompt gamma-ray emission lasting longer than 2 s – appear to be associated with the death of massive stars (e.g. Galama et al. 1998; Hjorth et al. 2003; Woosley & Bloom 2006; Hjorth & Bloom 2012). Meanwhile short GRBs (sGRBs) – GRBs with duration lasting less than about 2 s – are associated (at least in some cases) with the collision of two neutron stars or a neutron star and a black hole (Berger 2014; Fong et al. 2015; Abbott et al. 2017).

However, a number of recent results have called into question this general picture, and there still remain many open questions regarding the nature of both LGRB and sGRB progenitor systems. For example, recent observations suggest that some LGRBs may be a result of a double neutron star (DNS) merger based on a potential kilonova signal in their light curves, opening up the possibility that GRBs with prompt gamma-ray emission lasting 10s of seconds may indeed be produced by compact object binaries (Rastinejad et al. 2022; Troja et al. 2022; Yang et al. 2022b; Gottlieb et al. 2023; Levan et al. 2023; Yang et al. 2024). Additionally, recent studies using machine learning techniques to explore the classification of GRB progenitors (Dimple, Misra & Arun 2024; Zhu et al. 2024) have found that there may be significant 'contamination' or overlap between these two (i.e. short and LGRB) samples (this overlap had been pointed out previously, although in the context of suggesting a third class of GRBs; see e.g. Horváth & Tóth 2016).

Interestingly and potentially related to this issue, several studies have seen an uptick in the rate density of LGRBs at low redshifts (Petrosian, Kitanidis & Kocevski 2015; Yu et al. 2015; Le & Mehta 2017; Tsvetkova et al. 2017; Lloyd-Ronning, Aykutalp & Johnson 2019b; Le, Ratke & Mehta 2020; Lloyd-Ronning, Johnson & Aykutalp 2020b; Hasan & Azzam 2024; Petrosian & Dainotti 2024). Recently, Li et al. (2024) examined a subset of GRBs with extended emission and found they can be separated into two 'classes' or groups according to the slope and intercept of their $E_{\rm iso}$–E_p relation, where $E_{\rm iso}$ is the isotropic emitted energy and E_p is the peak of the prompt gamma-ray spectrum (see also Singh et al. 2024). Given their classifications, they find that the rate density of one subsample (which they name EE2) shows a strong increase at low redshifts while the other (subsample EE1) appears to more closely track the star formation rate (SFR; decreasing at low redshift). They interpret this as evidence of the presence of a distinctly different

★ E-mail: lloyd-ronning@lanl.gov
† Director's Postdoctoral Fellow.

progenitor at low redshifts (relative to the progenitor responsible for the EE1 subsample). Others have suggested that the low-redshift uptick may be due to the contribution from a compact object merger progenitor at these redshifts (Petrosian & Dainotti 2024), distinct from a system that more closely follows the SFR (e.g. a massive star). As such, it is important to consider the unique contribution of these compact object merger populations to the LGRB rate density.

There are a number of potential compact object merger systems that could contribute to the low-redshift uptick of the LGRB rate density, including DNS mergers, neutron star–black hole (NSBH) mergers, double white dwarf (WD) binary mergers, white dwarf–neutron star (WDNS) mergers, and white dwarf–black hole (WDBH) mergers. We have briefly discussed above the potential contribution from DNS and NSBH binary mergers; those systems remain viable contributors to the low-redshift uptick, although it is not easy to create the long-lived prompt gamma-ray emission in these scenarios due to the lack of available material in the disc around the central engine (e.g. Janiuk & Proga 2008).[1] Double WD binary mergers may be too weak, without enough material/fuel, to power an LGRB (see, e.g. Kremer et al. 2021; Yang, Thomas Tam & Yang 2022a). A WDNS binary merger has been suggested as a potential progenitor for at least one GRB (Zhong, Li & Dai 2023), as long as the WD component has a mass $> 1 M_{\odot}$ [on the other hand, Bobrick, Davies & Church (2017) has shown that for lower mass WDs the systems can survive and become ultracompact X-ray binaries]. The rates and delay time distributions (DTDs) of WDNS binaries are explored in detail in Toonen et al. (2018), who show these systems typically merge in < 1 Gyr and have a wide range of offsets from their host galaxies.[2] In principle, these systems may contribute to the low-redshift uptick of LGRBs, although rate estimates are uncertain.

In this paper, we explore how WDBH binary mergers contribute to the low-redshift uptick in the rate density of lGRBs. These models have been suggested as progenitors for LGRBs in a few studies (Fryer et al. 1999; Dong et al. 2018), but their population synthesis and contribution to the low-redshift population of LGRBs has not yet been fully scrutinized. We investigate the possibility that WD black hole mergers have the energetics, time-scales, and overall necessary rates to accommodate the uptick in the low-redshift rate density of GRBs.

Our paper is organized as follows. In Section 2, we recap the evidence that suggests a potential distinct population of low-redshift LGRBs, including an excess in the rate density at low redshifts. In Section 3, we summarize previous works and present order of magnitude calculations that show WDBH binaries have the necessary energetics and time-scales to power an LGRB. We also discuss the many factors that can play a role in their merger time-scales. In Section 4, we present results of population synthesis simulations that suggest that the rates of these systems per galaxy over a range of metallicities align with observational constraints. We provide analytic calculations of the WDBH rate density, using empirical estimates of DTDs of compact object mergers, and present the range of parameter space for which WDBH mergers can explain the low-redshift uptick in the observed rate density of LGRBs. Finally, we present a summary and our main conclusions in Section 5.

2 DATA

Fig. 1 shows the estimated or predicted SFR density from the observed GRB rate, relative to the global SFR as determined by Madau & Dickinson (2014) (black line):

$$\dot{\rho}_{\rm SFR\_GRBs}(z) = (\mathrm{d}\dot{N}/\mathrm{d}z)(\mathrm{f}_{\rm beam}(\mathrm{z}))\left(\frac{(1+z)}{\mathrm{d}V/\mathrm{d}z}\right)\frac{1}{\epsilon(z)}, \quad (1)$$

where $\mathrm{d}\dot{N}/\mathrm{d}z$ is the GRB rate (accounting for the GRB luminosity evolution and detector trigger selection effects), $\epsilon(z)$ parametrizes the fraction of stars that make GRBs (and in principle can evolve with redshift), and $f_{\rm beam}(z)$ is a factor (> 1) that accounts for the gamma-ray burst beaming angle (and its evolution with cosmic redshift; e.g. Lloyd-Ronning et al. 2019b). The factor $\mathrm{d}V/\mathrm{d}z$ is the cosmological volume element given by

$$\mathrm{d}V/\mathrm{d}z = 4\pi(\frac{c}{H_o})^3\left[\int_1^{1+z}\frac{d(1+z)}{\sqrt{\Omega_\Lambda+\Omega_m(1+z)^3}}\right]^2 \times\frac{1}{\sqrt{\Omega_\Lambda+\Omega_m(1+z)^3}}. \quad (2)$$

Removing the $1/\epsilon(z)$ factor, one can think of $\dot{\rho}_{\rm SFR\_GRBs}(z)$ as the rate density of GRB progenitor formation.

The cyan and blue lines show the rate density derived from observations of LGRBs, but without correcting for jet beaming angle evolution. The magenta and grey dashed region show the rate density, accounting for the fact the high-redshift GRBs may be more narrowly collimated than low-redshift GRBs (Lloyd-Ronning et al. 2020b); because in general we only observe the GRBs whose jets are pointed in our direction this means we are missing a higher fraction of GRBs in the high-redshift universe. The red dashed line is the rate density derived from observations of sGRBs [see also Dainotti, Petrosian & Bowden (2021) for a calculation of the rate density of sGRBs using non-parameteric methods]. The LGRB curves are normalized to the Madau & Dickinson (2014) SFR at its peak, while the sGRB curve is normalized to the SFR at a redshift of $(1+z) \sim 2$; this is an arbitrary choice, but attempts to account for the delay time between star formation and merger time in a DNS merger model for sGRBs (Nakar, Gal-Yam & Fox 2006; Berger et al. 2007; Hao & Yuan 2013a; Wanderman & Piran 2015; Anand, Shahid & Resmi 2018; Zevin et al. 2022).

Although accounting for the jet beaming angle evolution decreases the extent of the low-redshift uptick, it is still present in all cases for the LGRBs. The sGRB rate density, as expected, peaks at lower redshifts (most likely due to the time it takes the stars in this progenitor model to evolve and then merge). Again, the shape of the sGRB rate density seems to suggest that there might exist a contribution from compact object mergers to the low-redshift uptick in the LGRB population.

We note that, in this figure, the underlying GRB rate density – accounting for detector selection effects and luminosity evolution – was determined using the non-parametric statistical methods of Lynden-Bell (1971) and Efron & Petrosian (1992,1999). Others (Wanderman & Piran 2010; Lien et al. 2014; Pescalli et al. 2016) which have used parametric methods (which often makes an implicit assumption that the GRB rate follows the SFR more closely) see a smaller or no uptick at low redshifts.[3] Additionally, we note that

[1] This is under the assumption of a magnetically powered jet launched from a black hole-disc central engine.

[2] We note that 1 Gyr is shorter than the time between the peak of the SFR at $z \approx 2$ and the apparent uptick at $z < 1$.

[3] We note, however, that Lan et al. (2019) also used non-parametric methods to estimate the GRB rate density and luminosity function (including evolution) and found only a mild uptick at low redshifts, although their luminosity evolution agrees well with Lloyd-Ronning et al. (2019b).

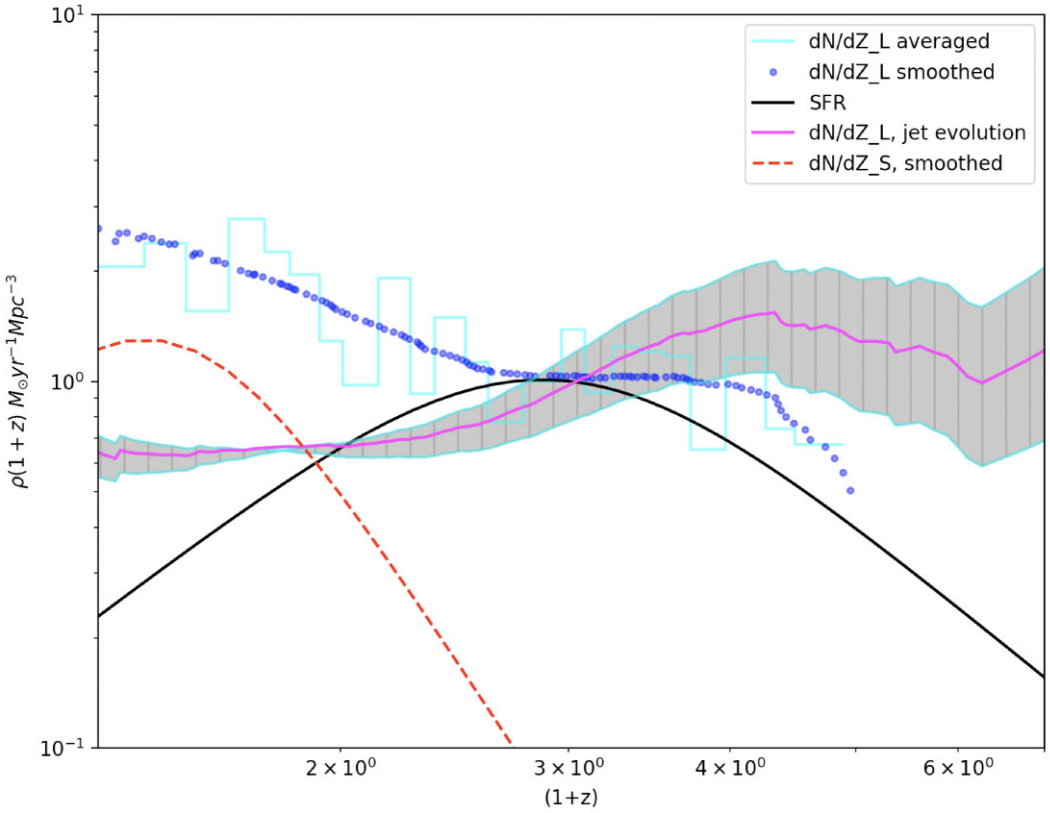

Figure 1. Long (L) GRB SFR density without accounting for jet opening angle evolution (cyan and blue curves), accounting for jet opening angle evolution (magenta and grey regions), and short (S) GRB rate density (red dashed curve). The black solid line indicates the SFR according to Madau & Dickinson (2014). The LGRB rate densities are normalized to the peak of the SFR at $(1+z) = 3$, while the sGRB rate density is normalized at a redshift of $(1+z) = 2$. As noted in Lloyd-Ronning et al. (2020b) the uptick at low redshifts is somewhat reduced if beaming angle evolution is accounted for.

if the formation efficiency of GRBs is drastically reduced at low redshifts (i.e. on average higher metallicities), this can also reduce the severity of the uptick and align the GRB rate density more closely with the SFR density (Perley et al. 2016). Finally, Lu et al. (2024) suggest that non-parametric methods can have degeneracies in the functional form of the underlying correlation so caution must be taken in drawing too strong of conclusions on the exact form of that function.

Given the possibility of a distinct population of low-redshift LGRBs, we have examined the isotropic energy distribution and duration of the prompt gamma-ray emission (corrected for time dilation) for the subset of bursts with $(1+z) < 2$. This cut-off is chosen simply because that is the redshift below which the deviation from the SFR begins to appear, though it does not necessarily delineate any GRB progenitor subpopulations in a robust way. We find the average value of $E_{\rm iso}$ is lower for this subset of low-redshift bursts relative to the whole population at a marginally statistically significant level (2.5σ). There is no statistically significant difference in the values of the durations between these samples. Again, this is not necessarily surprising because we have not attempted to delineate in any way the subsample of low-redshift LGRBs that maybe be coming from WDBH mergers and so there would be mixing between such a subsample and 'traditional' LGRBs that come from the collapse of massive stars.

As mentioned in the Introduction, Li et al. (2024) examined a population of GRBs with extended emission and found that this population could be further classified into two groups (which they named 'EE1' and 'EE2') based on the slope of the correlation between isotropic equivalent energy $E_{\rm iso}$ and the spectral peak energy E_p. Their EE2 subsample shows a rate density that is significantly enhanced at low redshifts, suggesting that perhaps this subsample originates from a distinct progenitor more prevalent at low redshifts.

We examined certain characteristics of the Li et al. (2024) EE1 and EE2 subsamples when the data were available, where – again – the former sample appears to follow the SFR while the latter exhibits an uptick at low redshifts relative to the SFR. We show the observed redshift distributions of their EE1 and EE2 samples in Fig. 2. We see that GRBs in their EE2 sample have significantly shorter prompt gamma-ray duration, shown in the left panel of Fig. 3. We also looked at the jet opening angles in their subsamples. There are 19 GRBs in their EE1 sample that have jet opening angle measurements, with a distribution that is not significantly different from the global LGRB population (Fig. 3, right panel). That only 2 GRBs in their EE2 sample had jet opening angle measurements could suggest a potentially much wider jet for this sample. However, many observational selection effects come into play when measuring jet opening angle and we simply do not have the numbers to test this hypothesis rigorously.

Based on studies that have suggested a dichotomy in progenitors between LGRBs with and without radio afterglows (Lloyd-Ronning & Fryer 2017; Lloyd-Ronning et al. 2019c; Chakraborty et al. 2023), we also looked at the presence or absence of radio

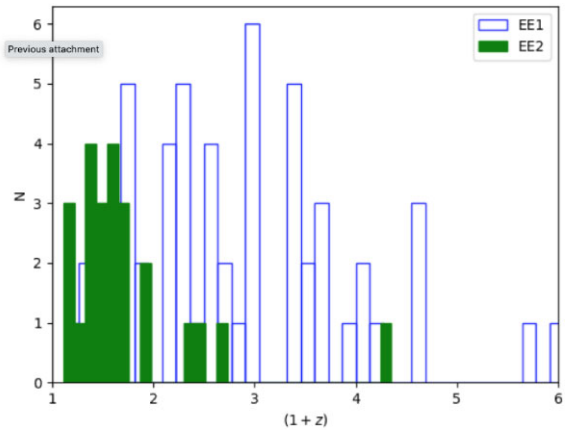

Figure 2. Observed redshift distribution of EE1 versus EE2 samples, as defined by Li et al. (2024). They suggest the EE2 sample may be coming from a distinct progenitor system compared to the EE1 sample.

emission in the EE1 and EE2 samples. Again, the numbers are small but we found that of those GRBs in the Li et al. (2024) samples that have a radio afterglow, 11 are from their EE1 subpopulation and only 1 is from the EE2 population. This is consistent with the conjecture that radio bright GRBs are the result of the collapse of a massive star in a dense gaseous environment (star-forming regions), while radio dark GRBs are in more tenuous environments as one might expect in a WDBH merger progenitor scenario.

If a low-redshift subpopulation of LGRBs might have a significant contribution from compact object binary merger progenitors, it is valuable to consider the host-galaxy offsets of low-redshift LGRBs, as compact object binary systems may receive a significant kick upon formation of the neutron star or black hole component (from the supernova that made it) and therefore tend to migrate well outside their host galaxies by the time they merge (and create the GRB). Meanwhile, massive star collapse progenitors tend to be found in the star-forming regions of their host galaxies, with relatively small offsets (Bloom, Kulkarni & Djorgovski 2002; Lyman et al. 2017). We might expect that if there exists a low-redshift population of LGRBs from compact object mergers, the host galaxy offsets of low-redshift GRBs may be on average slightly larger than those of high-redshift GRBs.

However, according to Blanchard, Berger & Fong (2016) there is no clear trend of host-galaxy offset with redshift for a sample of 100 or so LGRBs (see their fig. 4). When looking at the offsets of the Li et al. (2024) EE1 and EE2 samples, it is hard to draw any conclusions. The EE1 sample has only six offset measurements but having a look at the so-called EE1 and EE2 samples, there were six GRBs in the EE1 sample with offset measurements and with values 0.7, 0.81, 0.82, 1.73, 3.42, 5.20 kpc for the physical offset and 0.27, 0.3, 0.87, 1.09, 1.6, 3.425 for the normalized offset (normalized to the half-light ratio of the galaxy). These numbers appear to align with what is observed in LGRBs where most offsets appear to be within less than a few kpc or roughly within the half-light radii of their host galaxies (Bloom et al. 2002), as opposed to sGRBs, many of which have observed offsets that are 10s of kpc from the centre of their host galaxies (Fong et al. 2022). There is only one GRB in the EE2 sample that had an offset measurement, with values 0.992 kpc for the physical offset and 0.765 for the normalized offset. Hence, there is nothing in the sparse data to suggest any unusual trends with host-galaxy offset, although of course the small numbers make it difficult to draw any definitive conclusions about the existence or presence of a trend. We note that it is the supernova process with significant ejecta mass in addition to heavy element production that is believed to be responsible for large natal kick velocities in neutron stars (Wongwathanarat, Janka & Müller 2013; Bray & Eldridge 2016), Therefore, in general black holes may have smaller natal kick velocities than neutron stars (so that a large host galaxy offset may not be observed), although recent observations of mis-aligned spins from gravitational wave observations of black hole binaries have called this view into question (O'Shaughnessy, Gerosa & Wysocki 2017).

Putting all of this together, we suggest that a WDBH binary system may have the characteristics of both long and sGRBs, and be able to explain the trends (or lack thereof) in the data described above. In the next sections, we explore analytically and with population synthesis models the plausibility of a WDBH merger progenitor for LGRBs, and as a contributor to the low-redshift uptick in the LGRB rate density.

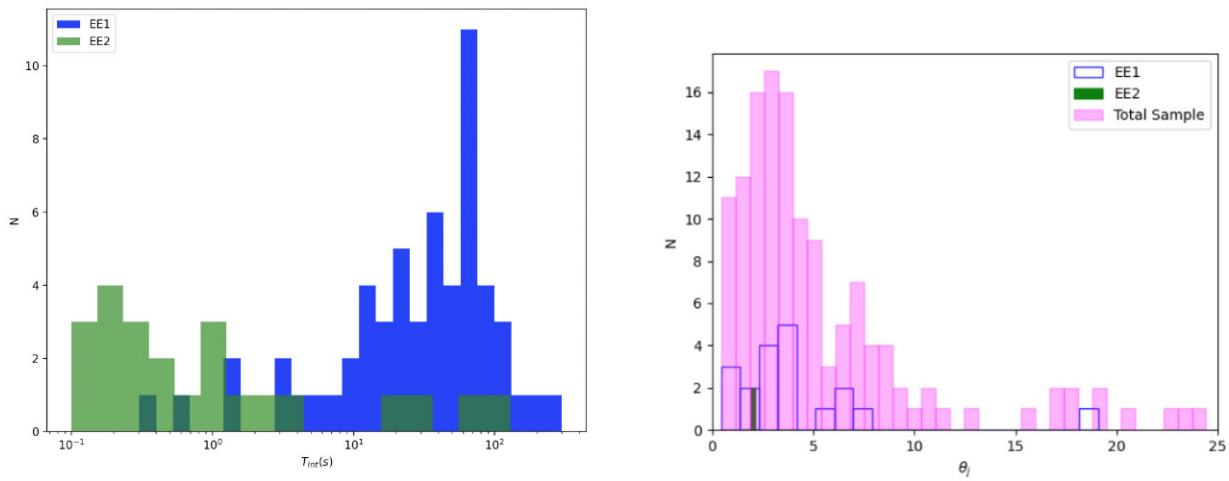

Figure 3. Left panel: Plot of intrinsic gamma-ray duration for the so-called EE1 (blue histogram) and EE2 (green histogram) samples from Li et al. (2024). The EE2 sample has a significantly shorter duration than the EE1 sample. Right panel: Plot of the jet opening angle for the EE1 (blue histogram) and EE2 samples (green histogram), as well as all LGRBs for which this data exist (pink histogram). Note that the EE2 sample has only a single jet opening angle measurement.

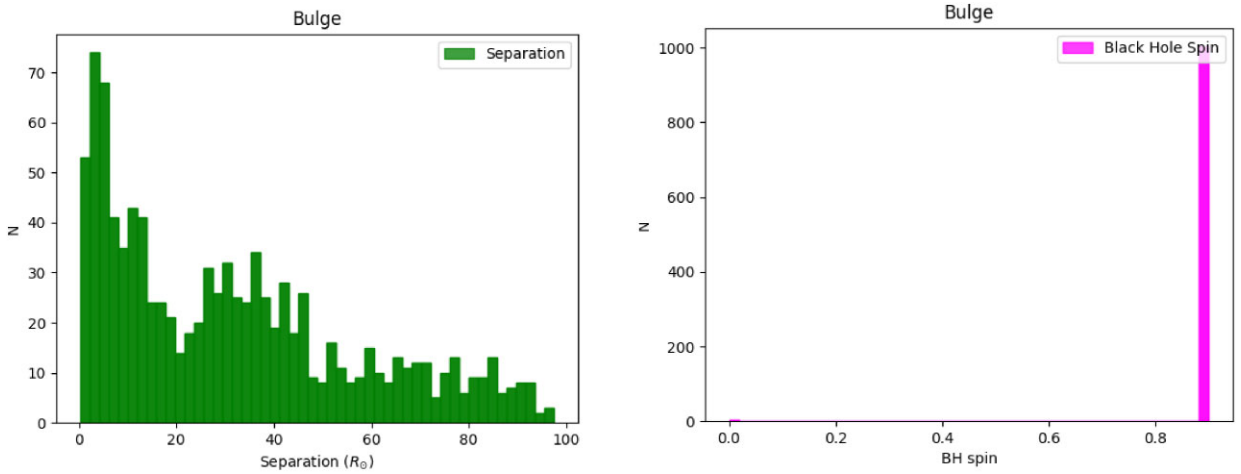

Figure 4. Distributions of WDBH binary separations (left panel) and spin of the black hole component (right panel), for a population synthesis simulation at metallicity $Z = 10^{-2}$. The y-axis has arbitrary normalization.

3 MODEL

3.1 Energetics and time-scales

In a WDBH merger model, the relativistic jet that produces GRB emission is launched from a black hole-accretion disc central engine that is formed when the WD overflows its Roche lobe and is tidally disrupted by the black hole, with its stellar material circularizing in a disc around the stellar mass black hole (for the physics of tidal disruption of a WD around massive black holes, see e.g. MacLeod et al. 2014; Lixin Dai, Lodato & Cheng 2021).

Fryer et al. (1999) provide analytic estimates, along with numerical SPH simulations, of the amount of material in the disc, the accretion rate, and the angular momentum in the disc. They find (using the equations of Eggleton 1983) that the WD is tidally disrupted when it reaches an orbital separation from the black hole between ∼3 and 5×10^9 cm, with nearly all of the mass of the WD circularizing (roughly about 1 $M_\odot$ of material) and an accretion rate of 0.05 $M_\odot$ s^{-1}.

Observations of GRBs require that the isotropic equivalent energies, $E_{\rm iso}$, lie in the range of 10^{50}–10^{54} erg. In reality, the energy released E_γ is concentrated in a relatively narrow jet and is closer to $\lesssim 10^{50}$ erg. In other words, $E_\gamma = E_{\rm iso}(1 - \cos(\theta_j))/2$, where θ_j is the opening angle of the jet. From an energy conservation standpoint alone, the orbital energy of the binary, the rotational energy of the black hole, and/or the mass energy of the WD are all sufficient energy reservoirs to account for the GRB energy budget. However, we need to consider in more detail how this energy is extracted from the system. A viable mechanism to is to have the WD material tidally disrupted and its material circularized in a jet around the black hole; magnetic fields in the disc will rapidly grow through the magnetorotational instability (Velikhov 1959; Chandrasekhar 1960; Acheson & Hide 1973; Balbus & Hawley 1991), and wind up (through frame-dragging) along the spin axis of the black hole. This can lead to a magnetically launched relativistic jet, which ultimately extracts the spin energy of the black hole through the so-called Blandford-Znajek (BZ) mechanism (Blandford & Znajek 1977; MacDonald & Thorne 1982). The luminosity of the jet is given by

$$L_{\rm BZ} = (k f c^5/64\pi G^2) a^2 \phi^2 M_{\rm BH}^{-2} \quad , \tag{3}$$

where k is a geometrical factor related to the magnetic field geometry (of order ~ 0.05), f is a factor of order unity, c is the speed of light, ϕ is the magnetic flux on the black hole, $a = Jc/GM_{\rm BH}^2$ is the black hole spin parameter, where J is the black hole angular momentum, and $M_{\rm BH}$ is the black hole mass $M_{\rm BH}$.

The jet power depends on the spin of the black hole, the magnetic flux, and the mass of the black hole, although we note the complicated interplay between all three of these variables. We can simplistically write down, under the assumption of flux conservation, the magnetic flux in terms of magnetic field strength B and mass of the black hole,[4] which leads us to the following expression for the observed jet luminosity (McKinney 2005; Tchekhovskoy, Narayan & McKinney 2010; Tchekhovskoy & Giannios 2015; Lloyd-Ronning et al. 2019a):

$$L_{\rm GRB} \approx 10^{50} {\rm erg} (\eta/0.1)(a/0.9)^2 (B/10^{16}{\rm G})^2 (M_{\rm BH}/5{\rm M}_\odot)^2 \tag{4}$$

and where we have used an efficiency factor η between the BZ jet power and the observed GRB jet luminosity, $L_{\rm GRB} = \eta L_{\rm BZ}$. Provided the disc can sustain the necessary magnetic flux[5] and the black hole spin is sufficient (with the spin parameter $\gtrsim 0.5$. Our population synthesis results described below show that the vast majority $>$ 90 per cent of the WDBH systems we simulated have a black hole spin parameter >0.8 (see the bottom right panel of Fig. 4), where we have used a prescription for the black hole spin based on the core mass as described in Belczynski et al. (2020).

We also require that the jet is sustained long enough to explain the duration of the prompt gamma-ray burst itself. The jet lifetime – which is directly correlated with the duration of the GRB prompt emission – is roughly proportional to the mass of the disc divided by the accretion rate:

$$T_{\rm jet} \approx M/\dot{M}. \tag{5}$$

Given that we have approximately a solar mass of material and using the estimate from Fryer et al. (1999) of an accretion rate

[4] $\phi \approx 4\pi B R^2$, where B is the magnetic field, and R is the Kerr radius given by $R = GM/c^2 + \sqrt{(GM/c^2)^2 - a^2}$.

[5] Many studies (Rosswog & Davies 2002; Price & Rosswog 2006; Obergaulinger, Aloy & Müller 2010; Tchekhovskoy, Narayan & McKinney 2011; Zrake & MacFadyen 2013; Morales Teixeira, Avara & McKinney 2018; Liska et al. 2018a; Liska, Tchekhovskoy & Quataert 2018b) have shown that indeed the disc can sustain a very high magnetic flux.

of about $5 \times 10^{-2} M_{\odot}/s$, this will allow for a roughly $20s$ GRB, well within the 'long' class of GRBs (duration $> 2s$). The accretion rate in this model is an uncertainty; for GRBs in general, studies have shown that accretion rates can span a wide range of values (Popham, Woosley & Fryer 1999; Kumar, Narayan & Johnson 2008; Tchekhovskoy & Giannios 2015; James, Janiuk & Nouri 2022; Janiuk & James 2022), from as low as $10^{-3}\,M_{\odot}\,s^{-1}$[6] (which will produce longer GRBs) to as high as $10\,M_{\odot}\,s^{-1}$ (which will produce shorter GRBs, for a given amount of material in the disc). In the WDBH model, again, we only have about $1\,M_{\odot}$ of material available (although this number can range from about 0.2–1.4$M_{\odot}$), but – given the large range of possible accretion rates – this still may accommodate GRBs ranging from subsecond up to hundreds (even thousands) of seconds. Hence, we suggest that this model can reasonably accommodate the durations of LGRBs.

3.2 Merger time-scale

A key factor when attempting to account for the apparent uptick of the low-redshift GRB rate density from a compact object merger progenitor is properly factoring in the delay time from the formation of the binary until the merger itself (when the GRB is produced). In other words, compact object merger populations – including WDBH mergers – are expected to follow the SFR *convolved with a DTD*.

However, this distribution is highly uncertain from a theoretical standpoint. It is a combination of the stellar evolution time-scale (i.e. the time for the system to form and evolve from the main sequence lifetimes of the stars in the binary), and the orbital decay time-scale until merger. This latter time-scale depends on what is causing the loss of orbital angular momentum in the system, which can happen through multiple channels. For example, gravitational wave emission (which depends on the masses of the binary components, their separation, and eccentricity) as well as losses due to gas and dynamical friction (which depends on a number of complicated environmental factors) can all contribute significantly to this time-scale.[7]

We define the merger time-scale as follows:

$$t_{\rm merge} = t_{\rm evolve} + \min(t_{\rm loss}), \tag{6}$$

where $t_{\rm evolve}$ is the time-scale for the WDBH system to form, and $\min(t_{\rm loss})$ is the shortest time-scale over which orbital angular momentum is lost up until the merger. The evolution times of these systems, as determined by our population synthesis simulations discussed in Section 4, are in general around a few hundred Myr. This is the time-scale, if the initial conditions permit, for a main sequence binary system to form a black hole and WD component, with the time-scale dominated by the stellar evolution of the lower mass star (i.e. the star that becomes the WD). However, we note that this is for the high end of the mass range of WDs ($> 1M_{\odot}$; this is to allow for sufficient material in the disc that forms during the merger and aligns with our estimates in Section 3. Lower mass stars will take much longer ($\sim$ 10 Gyr) to evolve and can provide a significant contribution to the WDBH population (and the delay time). The orbital angular momentum loss time-scales can span a wide range of values, and there are many different channels that contribute to this loss time-scale, including gravitational wave emission, common envelope evolution, mass-loss, dynamical friction, gas dynamical friction, and more. We discuss the contributions from a few of these channels below.

3.2.1 *Gravitational wave loss*

The loss time-scale due to gravitational wave emission is given by

$$t_{GW} \approx \frac{E_{\rm orb}}{{\rm d}E/{\rm d}t_{GW}}, \tag{7}$$

where $E_{\rm orb}$ is the orbital energy

$$E_{\rm orb} \approx G M_{\rm WD} M_{\rm BH}/r \tag{8}$$

and

$${\rm d}E/{\rm d}t_{GW} = \frac{32G^4(M_{\rm WD}+M_{\rm BH})M_{\rm WD}^2 M_{\rm BH}^2}{5c^5 r^5} f(e), \tag{9}$$

where $M_{\rm WD}$ is the mass of the WD, $M_{\rm BH}$ is the mass of the black hole, r is the separation, and $f(e)$ is a factor that depends on eccentricity which is of order 1. Combining equations (8) and (9), we find

$$t_{\rm GW} \approx \frac{5c^5 r^4}{32 f(e) G^3 (M_{\rm WD}+M_{\rm BH}) M_{\rm WD} M_{\rm BH}}. \tag{10}$$

This time-scale is highly dependent on separation. For a binary separation of 10 $R_{\odot}$, a 10 $M_{\odot}$ mass black hole, and 1 $M_{\odot}$ WD, this merger time due to gravitational wave radiation is $\approx 10^{11}$ yr (i.e. longer than the age of the universe). On the other hand, for a separation of a $0.1R_{\odot}$, this time-scale can be as short as about 10^3 yr. We have found in our population synthesis results (discussed below) that a significant fraction of these binaries tend to form at small $< R_{\odot}$ separations, although most of the population has separations $\geq R_{\odot}$. Therefore, given this very large time-scale to lose energy from gravitational wave emission for much of the WDBH population, it is crucial to consider other mechanisms that may lead the orbit to decay more quickly and merge within a Hubble time, and there are indeed a number of physical processes expected to contribute to this frictional loss time-scale.

For example, common envelope evolution is a widely accepted way of drastically reducing the orbital separation of a binary system and bringing a compact object binary merger time to within a Hubble time (e.g. Dominik et al. 2012; MacLeod, Ostriker & Stone 2018, we discuss this further below when we invoke a DTD for our WDBH mergers). Binaries embedded in a gaseous or densely populated environment can also lead to a drastic loss of orbital angular momentum and cause the binary system to merge well within a Hubble time (Zahn 2008; Rozner & Perets 2022; Rozner, Generozov & Perets 2023). The precise time-scale of these processes is system- and environment-dependent, and therefore can span a very large (and unconstrained) range, which we discuss briefly now.

3.2.2 *Dynamical friction*

Stars moving through a cluster with velocity v will experience deceleration in the direction of their motion from the gravitational forces of the other stars (Chandrasekhar 1943). The time-scale is the relaxation time of the system which is related to the total number of stars in a cluster N and the crossing time $t_{\rm cr} = R_{\rm sys}/{\rm v}$, where $R_{\rm sys}$ is

[6]This is particularly true in the Magnetically Arrested Disc (MAD) model in which magnetic flux built at the horizon halts the accretion onto the black hole; the jet is launched by the magnetic pressure which is sustained by the rotational energy of the black hole (Tchekhovskoy & Giannios 2015).

[7]For reference, we note the Keplerian time $t_{\rm orb} = (4\pi r^3/GM)^{1/2}$ is very short (< 1 yr) for separations r on the order 10s of solar radii and for a total mass M of the system of $10M_{\odot}$.

the size of the system, and is given by

$$\frac{N}{6\ln(N)} t_{\rm cr}. \quad (11)$$

For a velocity of $\sim 10^6 {\rm cm\,s^{-1}}$, a typical size of cluster 10^{20} cm, and $N \approx 1000$, this time-scale is 10s of Myr.

3.2.3 *Gas dynamical friction*

Ostriker (1999) computed the gas dynamical friction force on a body with mass M travelling at a velocity v through a uniform medium with mass density ρ. This drag is due to the gravitational force between the body and its wake, and can be expressed as

$$F = -l \times 4\pi\rho_{\rm gas}(GM)^2 {\rm v}^{-2}, \quad (12)$$

where l is an expression related to the Mach number $M_{\rm cs}$, and has limiting values $l \rightarrow M_{\rm cs}^3/3$ for $M_{\rm cs} << 1$, and $l \rightarrow ln({\rm v}t/r_{\rm min})$ for $M_{\rm cs} >> 1$. They found that this drag force is more efficient than the Chandrasekhar (1943) formula for dynamical friction in a collisionless medium as long as $M_{\rm cs} > 1$.

We note that Suzuguchi et al. (2024) has considered gas dynamical friction in a non-linear regime and find that in the subsonic gas, the gas dynamical friction can be even higher than what is estimated by linear theory while at higher Mach number, their results agree closely with linear theory. This means that we may get an even more rapid decay of the orbit than expected from the Ostriker (1999) results when in the subsonic regime.

3.2.4 *Magnetic braking*

Magnetic braking can also play a significant role in the loss of angular momentum of a binary system (Verbunt & Zwaan 1981). The system loses angular momentum due to the loss of mass from a magnetically coupled stellar wind, and significant decrease in the orbital angular momentum can happen on a time-scale of about 1 Gyr.

3.2.5 *Other loss processes*

There are some suggestions that dark matter density spikes exist around stellar mass black holes and can explain rapid orbital decay times (Chan & Lee 2023; Bertone 2024; Ireland 2024). Specifically, Kavanagh et al. (2020) show that a binary system evolving in various dark matter environments (dark matter spikes, cusps, mounds; Bertone 2024) would experience dynamical frictional similar to gaseous environments, leading to shorter orbital decay times. If one also models dark matter as an ultralight boson, then the dark matter can form quasi-bound states around black holes ('gravitational atoms', Baumann, Chia & Porto 2019). This opens the possibility for energy loss (and thus increased orbital decay rates) via 'ionization' of such bound states as the energy from a binary system is extracted to excite the lowest energy levels.

3.2.6. *Empirical estimates*

Given the numerous possibilities and vast parameter space (which is relatively unconstrained from first principles) for potential loss of angular momentum in a binary system, we need to consider other ways to constrain the merger time-scale. One avenue to do so is to use the estimated DTDs, inferred from observations of compact object binary mergers. A number of studies have attempted to constrain this distribution for neutron star mergers under the assumption that they are the progenitors of sGRBs (Nakar et al. 2006; Berger et al. 2007; Lee 2010; Hao & Yuan 2013a; Wanderman & Piran 2015; Anand et al. 2018; Belczynski et al. 2018; Chruslinska et al. 2018; Broekgaarden et al. 2022; Santoliquido et al. 2022). For example, Zevin et al. (2022), using observations of sGRBs, infer a power law for the DTD:

$$p(t_d) \propto t^{-\beta} \quad t_{\rm min} < t < t_{\rm max}, \quad (13)$$

where t_d is the delay time to merger. They find a $\beta = 1.83^{+0.35}_{-0.39}$, $t_{\rm min} = 184$ Myr, and $t_{\rm max} \gtrsim 7.4$ Gyr. They suggest that common envelope evolution and mass transfer in the binary are the primary physical reasons for the steepness of the DTD. Similarly, Maoz & Nakar (2024) constrained the DTD of NS binary systems using observations of recycled millisecond pulsars. They find that their sample can be divided into two populations: a so-called fast population in which the DTD $\propto t^{-1.9}$ and a slow population with the DTD $\propto t^{-1.1}$, with the former having an exponential cut-off below $t \sim 300$ Myr. Freundlich & Maoz (2021) used observations of Type Ia supernovae to constrain the DTD of double WD progenitor systems. Their best fit to the a power-law parametrization is also roughly t^{-1}.

In what follows, we use these empirical estimates of DTDs as a general guide to parametrize the DTD of WDBH binary mergers (although we allow for a wider range of parametrizations of the DTD), and subsequently estimate the WDBH rate density as a function of redshift.

4 POPULATION SYNTHESIS SIMULATIONS AND WDBH RATE DENSITY

We use the open-source code *Compact Object Synthesis and Monte Carlo Investigation Code* (COSMIC) to run our population synthesis calculations (Breivik et al. 2020). This code is specifically tailored for modelling binary systems, computing stellar evolution based on the equations of Hurley, Pols & Tout (2000) and binary interactions according to Hurley, Tout & Pols (2002), but includes extensive improvements to account for factors important for compact object formation, such as metallicity-dependent winds and black hole natal kick strength (for a detailed description of the updates, see Breivik et al. 2020). We note the Hurley et al. (2000) work develops an extensive set of equations to account for all stages of a star's evolution through the Hertzsprung–Russell diagram, across all masses and metallicities.

The initial sample of binary parameters (primary and secondary masses, orbital periods, eccentricities, metallicities, and star formation histories) is generated by randomly sampling distribution functions based on models described in Moe & Di Stefano (2017). They use a wide range of observational data to develop their models, and find an empirical relationship between mass ratio and orbital separation (with more modest ratios $q \sim 0.5$ for smaller orbital periods, while larger orbital periods seem to have mass ratios consistent with random sampling from the initial mass function), which is incorporated into the COSMIC code.

COSMIC has well-defined prescriptions to deal with binary mass transfer, common envelope evolution, winds, natal kicks, and other binary-specific evolution parameters, based on the equations laid out in Hurley et al. (2000) and Hurley et al. (2002). We adopt an Eddington-limited mass-transfer scheme, draw natal kicks from a bimodal distribution based on whether they go through an iron core-collapse supernova versus an electron-capture or ultrastripped supernova, and follow the wind prescription described in Vink & de Koter (2005). We have also employed a common envelope efficiency (defined as the efficiency of transferring orbital angular momentum

Table 1. Fraction of WDBH binaries to total number of stars for different metallicities from the population synthesis code COSMIC.

$n_{\rm WDBH}/n_{\rm stars}$	Z
$7\,(\pm1)\times10^{-7}$	0.001
$3\,(\pm1)\times10^{-6}$	0.005
$1\,(\pm1)\times10^{-6}$	0.01

into kinetic energy of the envelope) of 1. The onset of unstable mass transfer and common envelope evolution are determined by a critical mass ratio according to Hjellming & Webbink (1987).

COSMIC takes a Monte Carlo approach to sampling and evolving the population which allows for much faster and more efficient simulations. For our simulations described below we confirmed convergence, ensuring we sample sufficiently (and that our results do not depend on our computational set-up such as number of processors, threading, etc.).

We have run a suite of simulations over different initial conditions, focusing on systems in which the initial masses of the stars fall in the range of 1–80 $M_\odot$ and which evolve into WDBH binaries (we note the COSMIC convergence criteria are computed at the formation of the binary). For a given galaxy, we simulate a burst of star formation as well as constant star formation lasting 0.5 and 10 Gyr, over a range of metallicities. In Table 1, we provide the simulation output for three representative runs at three different metallicities, showing the fraction of WDBH systems relative to the total number of stars in the simulation.

We show the output for the binary separations and the black hole spin from a representative simulation at a metallicity of $Z = 10^{-2}$ in the left and right panels of Fig. 4, respectively. This simulation was run under the condition of a burst of star formation at a redshift of $z \approx 2$; we then allowed the population of stars evolve from that point to the present day. As mentioned previously, the black hole spin is calculated according to the prescription described in Belczynski et al. (2020). The y-axis shows un-scaled simulation numbers.[8] Fig. 5 shows the corresponding DTD, from the simulation although we caution that this distribution is solely based on loss of angular momentum due to gravitational wave radiation.

Our results indicate that the WDBH fraction per galaxy is $\lesssim 10^{-6}$ of the total number of stars for separations $r \leq 100R_\odot$, across a range of metallicities spanning $Z = 10^{-3}$ to $Z = 10^{-2}$. Interestingly, we find a slightly higher fraction of these systems for higher metallicity (although only very marginally so). This fraction decreases to about 3×10^{-8} if we only consider WDBH with $r \lesssim 2R_\odot$ (i.e. at a separation where gravitational radiation is enough to cause the merger within a Hubble time). We note that Fryer et al. (1999) estimates the rates of WDBH mergers to be between 10^{-9} and 10^{-6} yr^{-1} galaxy^{-1}. Dong et al. (2018), using results from Nelemans, Yungelson & Portegies Zwart (2001), quote a rate of about 2×10^{-6} yr^{-1} in the galactic disc, for systems with a typical black hole mass of about 5–7 $M_\odot$.

In principle, we can also estimate an upper limit to this rate using observations of the low-mass X-ray binary (LMXB) population. For example, if we take the average LMXB luminosity and use the scaling relation between total X-ray (in the range

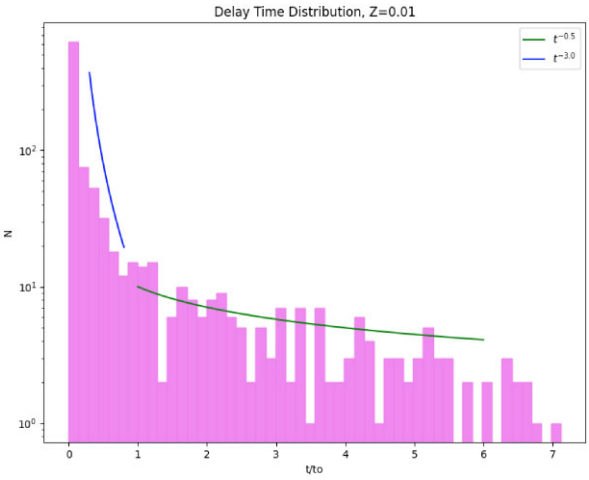

Figure 5. DTD for a population synthesis simulation at metallicity $Z = 10^{-2}$. The y-axis has arbitrary normalization. The blue line shows a DTD with a power-law index of -3, while the green line shows a power-law index of -0.5.

of 0.5–8 keV) LMXB luminosity per galaxy and stellar mass, $L_{\rm LMXB}/M_{\rm star} \sim 9 \times 10^{28}$ erg s^{-1} $M_\odot^{-1}$ (Gilfanov, Grimm & Sunyaev 2004; Lehmer et al. 2010; Upton Sanderbeck et al. 2018), we can roughly estimate the number of LMXBs for a given stellar mass. Fig. 12 of Grimm, Gilfanov & Sunyaev (2002) shows the luminosity function of LMXBs, which can vary across several orders of magnitude Fabbiano (2006). Recent observations of LMXBs in our galaxy have catalogued roughly ~ 300 LMXBs in the Milky Way (e.g. Avakyan et al. 2023; Fortin et al. 2024). However, this number is difficult to pin down and likely a lower limit because of the transient nature of these systems as well as accounting for detector sensitivity limits, but it can help guide our rate estimates in principle, keeping in mind the WDBH population is only a fraction of the LMXB population.

4.1 WDBH rate density

Ultimately, we are trying to understand if the uptick at low redshifts in the rate density of LGRBs (shown by the cyan, blue, and magenta lines in Fig. 1) can be explained by WDBH mergers, under the assumption that the WDBH merger rate density follows the SFR *convolved with a DTD*, which accounts for the time between formation of the system and merger.

Our approach to estimating this is as follows:

(i) For a given so-called birth redshift, $z_{\rm birth}$, of a WDBH system, we draw a sample of 1000 delay times from a DTD as parametrized in equation (13), with a power-law index β and a minimum delay time $t_{\rm min}$.[9]

(ii) For each delay time, we compute the corresponding redshift at which the merger would occur, $z_{\rm merge}$, the upper limit of the following integral:

$$t_d = -\frac{1}{H_o}\int_{z_{\rm birth}}^{z_{\rm merge}} \frac{{\rm d}z}{(1+z)E(z)}, \tag{14}$$

[8]To scale to an astrophysical population, we need to multiply the fraction of our WDBHs by the total number of stars in a given galaxy. For the purposes of this paper, we remain agnostic to this number (i.e. the number of stars in any particular galaxy).

[9]It is important to take care when transforming from time to redshift space; a given merger delay time will correspond to a different redshift delay at different redshifts.

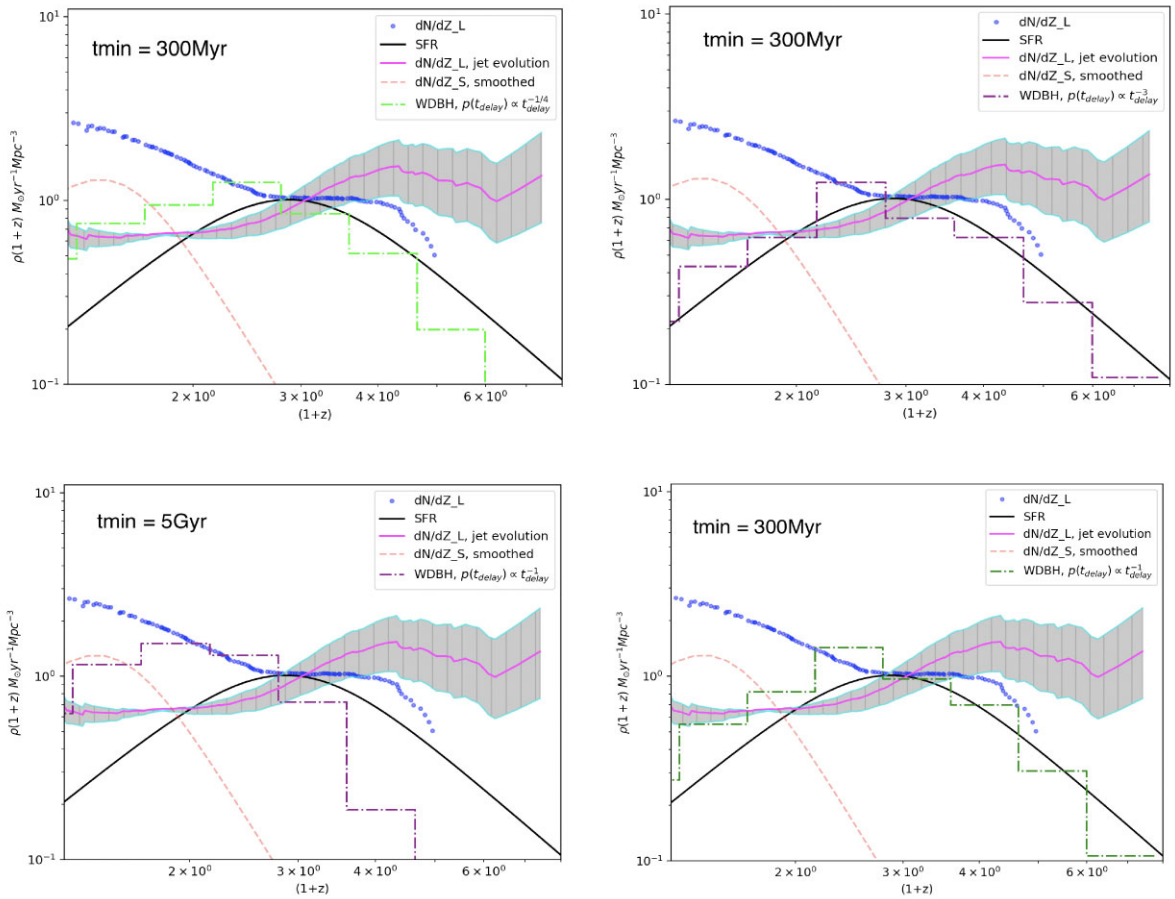

Figure 6. Same as Fig. 1, but now we have included our theoretical estimates for the contribution from the WDBH merger population that could produce GRBs (dash–dotted histograms). Top panels: The left panel shows our predictions for the WDBH rate density for a very flat DTD with a power law index of $\beta = 1/4$ [see equation (13) for the definition of β], while the right panel shows the results for a steep DTD with a power law index $\beta = 3$. Both DTDs have a minimum cut-off time of $t_{\rm min} = 300$ Myr. It is clear only the flattest/shallowest DTDs can account for a significant uptick, for this value of $t_{\rm min}$. Bottom panels**:** Both panels show results using a DTD with a power law index of $\beta = 1$, but the left bottom panel has a minimum cut-off time of 5 Gyr, compared to 300 Myr for the right panel. As expected, a larger $t_{\rm min}$ produces a much greater excess of these systems at low redshift.

where $E(z)$ is given by

$$E(z) = \sqrt{\Omega_m(1+z)^3 + \Omega_\Lambda} \tag{15}$$

and where we use an H_o of 70 km s^{-1} Mpc^{-1}, $\Omega_m = 0.3$, and $\Omega_\Lambda = 0.7$.

(iii) We now have a distribution of where WDBH mergers will occur for a given birth redshift, for a particular DTD. We then normalize this distribution by the SFR of Madau & Dickinson (2014) at the birth redshift, $\rho_{\rm SFR}(z_{\rm birth})$. Note that we do not make any corrections for jet opening angle evolution; this is because we have no a priori theoretical or observational constraints on this factor for WDBH merger systems. This is contrast to LGRBs resulting from the collapse of massive stars where it is expected that the dense stellar envelope and cocoon environment around the black hole disc system will collimate the jet as it emerges into the medium beyond the stellar envelope and radiates (Lloyd-Ronning et al. 2020a).

(iv) We repeat the steps above for a series of birth redshifts ranging from 10 to 0.5, and then integrate all of the SFR weighted distributions over birth redshifts to get the final total rate density of where the WDBH merger occurs.

Our results are shown in Figs 5 and 6, for a range of potential DTDs for the WDBH systems. In particular, we allow for a relatively wide range in the power-law index β and minimum delay time t_{min}. The top panels of Fig. 6 show a DTD with a $\beta = 1/4$ (left panel) and $\beta = 3$ (right panel). As expected, the flatter DTDs lead to a larger number of systems at low redshift – an excess compared to the SFR at these redshifts. Both of the bottom panels of Fig. 6 show results utilizing a DTD with a $\beta = 1$, but with different minimum delay times. The left panel, with a 5 Gyr minimum delay time, shows a strong excess in the rate density compared to the SFR at low redshifts, while the right panel, with a 300 Myr delay time, shows a smaller excess.

We note that shallow DTDs (i.e. low values of β) may be well-justified not only because these DTDs are currently very unconstrained, but also because a significant fraction of these systems could form by dynamical capture, as is believed to be the case for LMXBs in globular clusters, for example. This could serve to flatten the DTD and also increase the value of $t_{\rm min}$. A large value of $t_{\rm min}$ is also motivated simply by the fact that it can take a few Gyr for a lower-mass star to form the WD component of the system.

The green region of Fig. 7 highlights the range of parameter space where the WDBH merger systems produce an uptick at low redshifts compared to the SFR. This shaded region covers the range of parameter space for the DTDs shown in Fig. 7.

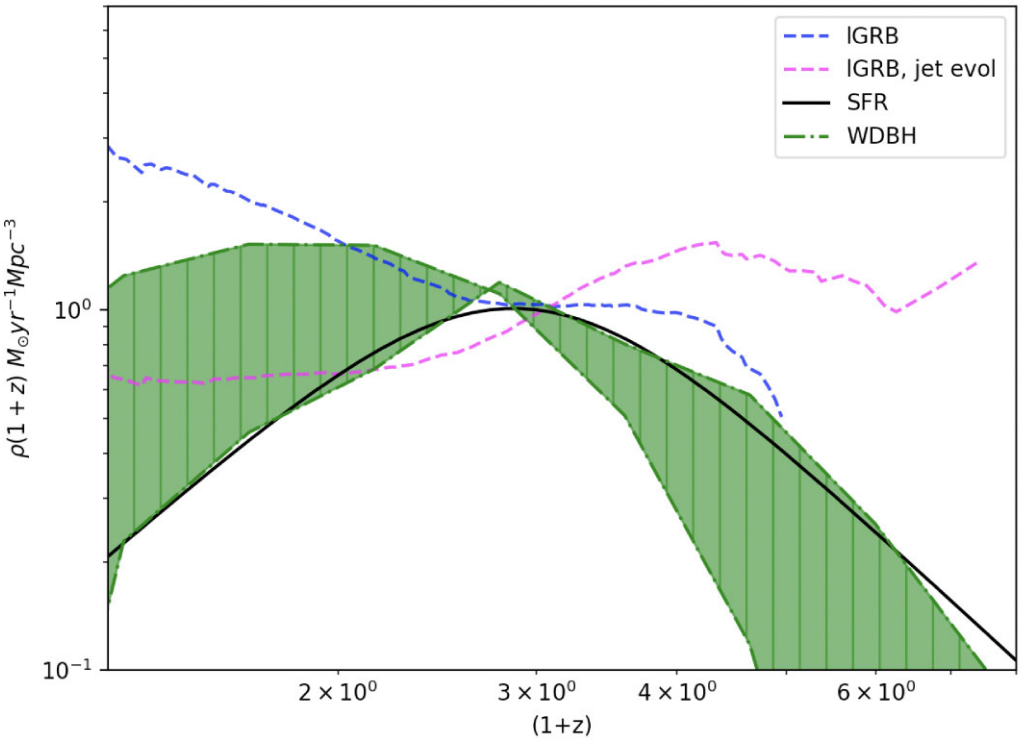

Figure 7. Same as Figs 1 and 5, but showing only the SFR (black line), the rate density from LGRBs (blue dashed line and magenta line, where the latter corrects for jet opening angle evolution), and a the contribution from WDBH merger systems for a reasonably motivated range of parameter space for the DTDs (green region), as discussed in the text.

The dashed lines are the LGRB rate density with and without correcting for beaming angle evolution (blue and magenta lines, respectively). It appears that under our assumptions, at least some of the low-redshift uptick (all, in the case of the beaming-angle-evolution corrected rate density) can be accommodated by WDBH mergers.

5 CONCLUSIONS

In this paper, we have investigated the viability of a WDBH merger progenitor for LGRBs, particularly focusing on its contribution to the apparent low-redshift uptick in the GRB rate density. We have scrutinized how a WDBH merger system can fulfil the necessary observational constraints of LGRBs, specifically the time-scales of the prompt emission, the overall energetics, and the rate density. Our main results are as follows:

(i) We have provided basic analytic arguments showing that a WDBH merger system fulfils the necessary energy and time-scale requirements for an LGRB. In particular, if most of the mass of the WD is tidally disrupted by its black hole companion and circularized into a disc around a massively spinning black hole, the central engine will be luminous enough and last long enough to power an LGRB.

(ii) We have discussed the many channels of orbital angular momentum loss and connected this to the merger time of the WDBH system, which is ultimately responsible for any deviation of their rate density from the SFR. We have shown that this time-scale is not well-constrained from first principles, but that constraints from observations of other compact object mergers (e.g. DNS binaries) may be a useful guide when estimating the WDBH DTD.

(iii) We have run a suite of population synthesis codes across metallicities to estimate the fraction of these systems in a given galaxy, relative to the total stellar population. We find this fraction ($\sim 10^{-8}$–10^{-6}) aligns with previously published estimates. We again emphasize we have only focused on systems with WDs that lie on the high end of the mass distribution ($\geq 1M_\odot$).

(iv) Guided by previously published DTDs for compact object binaries, we estimate the rate density of WDBH mergers and find that for relatively flat DTDs (with a power-law index ranging from $\beta \sim 2$ to $\sim 1/4$) and/or a minimum delay time above of a few hundred Myr to a few Gyr, these systems can explain the apparent low-redshift uptick in the LGRB rate density. Even under conservative assumptions for their DTDs, WDBH mergers can account for the beaming-angle-evolution-corrected low-redshift rate density. The more severe uptick seen in the uncorrected LGRB rate density can be explained by WDBH mergers with shallow DTDs and/or long minimum cut-off times.

We hope to further test this WDBH progenitor model as we obtain more data, in particular examining whether this potential low-redshift subpopulation of GRBs may be preferentially radio dark, have a unique gamma-ray duration distribution, jet opening angle distribution, and/or larger galaxy offsets on average. Another unique signature may come from quasi-periodic modulations in the light curves, resulting from repeated partial disruptions of these events (Chen et al. 2024). Future gravitational wave observations, both with ground-based observatories like LVK (Abbott et al. 2020) and Cosmic Explorer (Ng et al. 2021), as well as space-based observatories including LISA (Sberna, Toubiana & Miller 2021) and higher frequency decihertz gravitational wave detectors like DECIGO (Seto, Kawamura & Nakamura 2001; Kinugawa et al.

2022) and TianGO (Kuns et al. 2020), may uncover the population of WDBH binaries and directly test their connection to LGRBs as well.

Church et al. (2017) has shown that for WDBH binaries to merge, the mass ratio in the binary must be larger than about 0.2, meaning these systems will merge primarily for black hole masses $\lesssim 8M_{\odot}$. In subsequent papers (Zenati, Bobrick & Perets 2020; Bobrick et al. 2022), they suggest that both WDNS and WDBH systems may be accompanied by a faint optical transient, potentially detectable by deep follow-up observations of GRBs. On the other hand, we note an important point when considering this model for GRBs with an observed kilonova signal: Metzger (2012), Margalit & Metzger (2016), and Fernández, Margalit & Metzger (2019) have shown that neither WDNS mergers nor WDBH mergers have sufficient material nor the accretion rate to produce a kilonova signal in the light curve (also noted in Bobrick et al. 2022, for WDNS mergers). In particular, in their calculations, the accretion rate does not exceed a critical value of ($\sim 10^{-2}M_{\odot}/s$) necessary for *r*-process elements to be produced in the disc-wind ejecta. As such, we may in fact rule out the WDBH progenitor for those GRBs with a kilonova signal in their light curves.

As mentioned in Section 2, some studies (e.g. Perley et al. 2016) have suggested that if a metallicity dependent factor is included in the formation efficiency of LGRBs (where it is assumed that GRBs form more readily in low-metallicity environments), the GRB rate density more closely tracks the SFR at low redshifts. Although theoretical (e.g. Hirschi, Meynet & Maeder 2005; Woosley & Heger 2006; Yoon, Langer & Norman 2006) and observational (e.g. Graham & Fruchter 2013, 2017) studies have suggested LGRBs favour low-metallicity environments, there remain many open questions regarding the details of the exact metallicity requirements. Indeed, some LGRBs have been observed in high-metallicity environments (Levesque et al. 2010; Elliott et al. 2012; Krühler et al. 2012; Savaglio et al. 2012; Elliott et al. 2013; Hao & Yuan 2013b), and it is unclear if and how to account for a metallicity cut-off in a definitive and accurate way.

None the less, regardless of the presence of the low-redshift uptick in the LGRB rate density, we would argue that the study of the contribution of compact object binary progenitors to the LGRB population can help us home in on important factors in the evolution of these systems, as well as better understand the varied GRB progenitor landscape.

ACKNOWLEDGEMENTS

We are very grateful to the anonymous referee for helpful comments that improved this manuscript. We thank Ayanah Cason, Lailani Kenoly, Katie Breivik, Vera Delfavero, Mike Zevin, Gabriel Casabona, and Shane Larson for helpful discussions related to *COSMIC* simulations. We also thank Brian Metzger and Alexey Bobrick for insightful comments and suggestions. This work was supported by the U.S. Department of Energy through Los Alamos National Laboratory (LANL). LANL is operated by Triad National Security, LLC, for the National Nuclear Security Administration of U.S. Department of Energy (Contract No. 89233218CNA000001). Research presented was supported by the Laboratory Directed Research and Development programme of LANL project number 20230115ER. We acknowledge LANL Institutional Computing HPC Resources under project w23extremex. Additional research presented in this article was supported by the Laboratory Directed Research and Development programme of Los Alamos National Laboratory under project number 20210808PRD1 with report number LA-UR-24-28685.

DATA AVAILABILITY

The data generated and used in this paper are available upon request.

REFERENCES

Abbott B. P. et al., 2017, Phys. Rev. Lett., 119, 161101
Abbott B. P. et al., 2020, Living Rev. Rel., 23, 3
Acheson D. J., Hide R., 1973, Rep. Prog. Phys., 36, 159
Anand N., Shahid M., Resmi L., 2018, MNRAS, 481, 4332
Avakyan A., Neumann M., Zainab A., Doroshenko V., Wilms J., Santangelo A., 2023, A&A, 675, A199
Balbus S. A., Hawley J. F., 1991, ApJ, 376, 214
Baumann D., Chia H. S., Porto R. A., 2019, Phys. Rev. D, 99, 044001
Belczynski K. et al., 2018, preprint (arXiv:1812.10065)
Belczynski K. et al., 2020, A&A, 636, A104
Berger E., 2014, ARA&A, 52, 43
Berger E. et al., 2007, ApJ, 664, 1000
Bertone G., 2024, Nucl. Phys. B, 1003, 116487
Blanchard P. K., Berger E., Fong W.-f., 2016, ApJ, 817, 144
Blandford R. D., Znajek R. L., 1977, MNRAS, 179, 433
Bloom J. S., Kulkarni S. R., Djorgovski S. G., 2002, AJ, 123, 1111
Bobrick A., Davies M. B., Church R. P., 2017, MNRAS, 467, 3556
Bobrick A., Zenati Y., Perets H. B., Davies M. B., Church R., 2022, MNRAS, 510, 3758
Bray J. C., Eldridge J. J., 2016, MNRAS, 461, 3747
Breivik K. et al., 2020, ApJ, 898, 71
Broekgaarden F. S. et al., 2022, MNRAS, 516, 5737
Chakraborty A., Dainotti M., Cantrell O., Lloyd-Ronning N., 2023, MNRAS, 520, 5764
Chan M. H., Lee C. M., 2023, ApJ, 943, L11
Chandrasekhar S., 1943, ApJ, 97, 255
Chandrasekhar S., 1960, Proc. Natl. Acad. Sci., 46, 253
Chen J., Shen R.-F., Tan W.-J., Wang C.-W., Xiong S.-L., Chen R.-C., Zhang B.-B., 2024, ApJ, 973, 33
Chruslinska M., Belczynski K., Klencki J., Benacquista M., 2018, MNRAS, 474, 2937
Church R. P., Strader J., Davies M. B., Bobrick A., 2017, ApJ, 851, L4
Dainotti M. G., Petrosian V., Bowden L., 2021, ApJ, 914, L40
Dimple, Misra K., Arun K. G., 2024, ApJ, 974, 55
Dominik M., Belczynski K., Fryer C., Holz D. E., Berti E., Bulik T., Mandel I., O'Shaughnessy R., 2012, ApJ, 759, 52
Dong Y.-Z., Gu W.-M., Liu T., Wang J., 2018, MNRAS, 475, L101
Efron B., Petrosian V., 1992, ApJ, 399, 345
Efron B., Petrosian V., 1999, J. Am. Stat. Assoc., 94, 824
Eggleton P. P., 1983, ApJ, 268, 368
Elliott J., Greiner J., Khochfar S., Schady P., Johnson J. L., Rau A., 2012, A&A, 539, A113
Elliott J. et al., 2013, A&A, 556, A23
Fabbiano G., 2006, ARA&A, 44, 323
Fernández R., Margalit B., Metzger B. D., 2019, MNRAS, 488, 259
Fong W., Berger E., Margutti R., Zauderer B. A., 2015, ApJ, 815, 102
Fong W.-f. et al., 2022, ApJ, 940, 56
Fortin F., Kalsi A., García F., Simaz-Bunzel A., Chaty S., 2024, A&A, 684, A124
Freundlich J., Maoz D., 2021, MNRAS, 502, 5882
Fryer C. L., Woosley S. E., Herant M., Davies M. B., 1999, ApJ, 520, 650
Galama T. J. et al., 1998, Nature, 395, 670
Gilfanov M., Grimm H. J., Sunyaev R., 2004, MNRAS, 347, L57
Gottlieb O. et al., 2023, ApJ, 958, L33
Graham J. F., Fruchter A. S., 2013, ApJ, 774, 119
Graham J. F., Fruchter A. S., 2017, ApJ, 834, 170
Grimm H. J., Gilfanov M., Sunyaev R., 2002, A&A, 391, 923
Hao J.-M., Yuan Y.-F., 2013a, A&A, 558, A22

Hao J.-M., Yuan Y.-F., 2013b, ApJ, 772, 42
Hasan A. M., Azzam W. J., 2024, Int. J. Astron. Astrophys., 14, 20
Hirschi R., Meynet G., Maeder A., 2005, A&A, 443, 581
Hjellming M. S., Webbink R. F., 1987, ApJ, 318, 794
Hjorth J., Bloom J. S., 2012, Cambridge Astrophysics Series 51, Gamma-Ray Bursts. p. 169
Hjorth J. et al., 2003, Nature, 423, 847
Horváth I., Tóth B. G., 2016, Ap&SS, 361, 155
Hurley J. R., Pols O. R., Tout C. A., 2000, MNRAS, 315, 543
Hurley J. R., Tout C. A., Pols O. R., 2002, MNRAS, 329, 897
Ireland A., 2024, preprint (arXiv:2406.07624)
James B., Janiuk A., Nouri F. H., 2022, ApJ, 935, 176
Janiuk A., James B., 2022, A&A, 668, A66
Janiuk A., Proga D., 2008, ApJ, 675, 519
Kavanagh B. J., Nichols D. A., Bertone G., Gaggero D., 2020, Phys. Rev. D, 102, 083006
Kinugawa T., Takeda H., Tanikawa A., Yamaguchi H., 2022, ApJ, 938, 52
Kremer K., Rui N. Z., Weatherford N. C., Chatterjee S., Fragione G., Rasio F. A., Rodriguez C. L., Ye C. S., 2021, ApJ, 917, 28
Krühler T. et al., 2012, ApJ, 758, 46
Kumar P., Narayan R., Johnson J. L., 2008, MNRAS, 388, 1729
Kuns K. A., Yu H., Chen Y., Adhikari R. X., 2020, Phys. Rev. D, 102, 043001
Lan G.-X., Zeng H.-D., Wei J.-J., Wu X.-F., 2019, MNRAS, 488, 4607
Le T., Mehta V., 2017, ApJ, 837, 17
Le T., Ratke C., Mehta V., 2020, MNRAS, 493, 1479
Lee C.-H., 2010, J. Korean Phys. Soc., 56, 1619
Lehmer B. D., Alexander D. M., Bauer F. E., Brandt W. N., Goulding A. D., Jenkins L. P., Ptak A., Roberts T. P., 2010, ApJ, 724, 559
Levan A. J. et al., 2023, Nat. Astron., 7, 976
Levesque E. M., Kewley L. J., Graham J. F., Fruchter A. S., 2010, ApJ, 712, L26
Li Q. M., Sun Q. B., Zhang Z. B., Zhang K. J., Long G., 2024, MNRAS, 527, 7111
Lien A., Sakamoto T., Gehrels N., Palmer D. M., Barthelmy S. D., Graziani C., Cannizzo J. K., 2014, ApJ, 783, 24
Liska M., Tchekhovskoy A., Ingram A., van der Klis M., 2019, MNRAS, 487, 550
Liska M. T. P., Tchekhovskoy A., Quataert E., 2020, MNRAS, 494, 3656
Lixin Dai J., Lodato G., Cheng R. M., 2021, Space Sci. Rev., 217, 12
Lloyd-Ronning N. M., Fryer C. L., 2017, MNRAS, 467, 3413
Lloyd-Ronning N. M., Fryer C., Miller J. M., Prasad N., Torres C., Martin P., 2019a, MNRAS, 485, 203
Lloyd-Ronning N. M., Aykutalp A., Johnson J. L., 2019b, MNRAS, 488, 5823
Lloyd-Ronning N. M., Gompertz B., Pe'er A., Dainotti M., Fruchter A., 2019c, ApJ, 871, 118
Lloyd-Ronning N., Hurtado V. U., Aykutalp A., Johnson J., Ceccobello C., 2020a, MNRAS, 494, 4371
Lloyd-Ronning N. M., Johnson J. L., Aykutalp A., 2020b, MNRAS, 498, 5041
Lu R.-J., Chen W.-H., Liang W.-Q., Peng C.-F., 2024, MNRAS, 529, 4523
Lyman J. D. et al., 2017, MNRAS, 467, 1795
Lynden-Bell D., 1971, MNRAS, 155, 95
MacDonald D., Thorne K. S., 1982, MNRAS, 198, 345
MacLeod M., Goldstein J., Ramirez-Ruiz E., Guillochon J., Samsing J., 2014, ApJ, 794, 9
MacLeod M., Ostriker E. C., Stone J. M., 2018, ApJ, 863, 5
Madau P., Dickinson M., 2014, ARA&A, 52, 415
Maoz D., Nakar E., 2024, preprint (arXiv:2406.08630)
Margalit B., Metzger B. D., 2016, MNRAS, 461, 1154
McKinney J. C., 2005, ApJ, 630, L5
Metzger B. D., 2012, MNRAS, 419, 827
Moe M., Di Stefano R., 2017, ApJS, 230, 15
Morales Teixeira D., Avara M. J., McKinney J. C., 2018, MNRAS, 480, 3547
Nakar E., Gal-Yam A., Fox D. B., 2006, ApJ, 650, 281
Nelemans G., Yungelson L. R., Portegies Zwart S. F., 2001, A&A, 375, 890
Ng K. K. Y., Vitale S., Farr W. M., Rodriguez C. L., 2021, ApJ, 913, L5
O'Shaughnessy R., Gerosa D., Wysocki D., 2017, Phys. Rev. Lett., 119, 011101
Obergaulinger M., Aloy M. A., Müller E., 2010, A&A, 515, A30
Ostriker E. C., 1999, ApJ, 513, 252
Perley D. A. et al., 2016, ApJ, 817, 7
Pescalli A. et al., 2016, A&A, 587, A40
Petrosian V., Dainotti M. G., 2024, ApJ, 963, L12
Petrosian V., Kitanidis E., Kocevski D., 2015, ApJ, 806, 44
Popham R., Woosley S. E., Fryer C., 1999, ApJ, 518, 356
Price D. J., Rosswog S., 2006, Science, 312, 719
Rastinejad J. C. et al., 2022, Nature, 612, 223
Rosswog S., Davies M. B., 2002, MNRAS, 334, 481
Rozner M., Perets H. B., 2022, ApJ, 931, 149
Rozner M., Generozov A., Perets H. B., 2023, MNRAS, 521, 866
Santoliquido F., Mapelli M., Artale M. C., Boco L., 2022, MNRAS, 516, 3297
Savaglio S. et al., 2012, MNRAS, 420, 627
Sberna L., Toubiana A., Miller M. C., 2021, ApJ, 908, 1
Seto N., Kawamura S., Nakamura T., 2001, Phys. Rev. Lett., 87, 221103
Singh D., Singh M., Verma D., Lal Pandey K., Gupta S., 2024, preprint (arXiv:2406.15993)
Suzuguchi T., Sugimura K., Hosokawa T., Matsumoto T., 2024, ApJ, 966, 7
Tchekhovskoy A., Giannios D., 2015, MNRAS, 447, 327
Tchekhovskoy A., Narayan R., McKinney J. C., 2010, ApJ, 711, 50
Tchekhovskoy A., Narayan R., McKinney J. C., 2011, MNRAS, 418, L79
Toonen S., Perets H. B., Igoshev A. P., Michaely E., Zenati Y., 2018, A&A, 619, A53
Troja E. et al., 2022, Nature, 612, 228
Tsvetkova A. et al., 2017, ApJ, 850, 161
Upton Sanderbeck P. R., McQuinn M., D'Aloisio A., Werk J. K., 2018, ApJ, 869, 159
Velikhov E., 1959, Sov. Phys. JETP, 36, 995
Verbunt F., Zwaan C., 1981, A&A, 100, L7
Vink J. S., de Koter A., 2005, A&A, 442, 587
Wanderman D., Piran T., 2010, MNRAS, 406, 1944
Wanderman D., Piran T., 2015, MNRAS, 448, 3026
Wongwathanarat A., Janka H. T., Müller E., 2013, A&A, 552, A126
Woosley S., Bloom J., 2006, Annu. Rev. Astron. Astrophys., 44, 507
Woosley S. E., Heger A., 2006, ApJ, 637, 914
Yang H.-W., Thomas Tam P.-H., Yang L., 2022a, Res. Astron. Astrophys., 22, 105014
Yang J. et al., 2022b, Nature, 612, 232
Yang Y.-H. et al., 2024, Nature, 626, 742
Yoon S.-C., Langer N., Norman C., 2006, A&A, 460, 199
Yu H., Wang F. Y., Dai Z. G., Cheng K. S., 2015, ApJS, 218, 13
Zahn J. P., 2008, in Goupil M. J., Zahn J. P.eds, EAS Publications Series, Vol. 29, Tidal Effects in Stars, Planets and Disks. p. 67
Zenati Y., Bobrick A., Perets H. B., 2020, MNRAS, 493, 3956
Zevin M., Nugent A. E., Adhikari S., Fong W.-f., Holz D. E., Kelley L. Z., 2022, ApJ, 940, L18
Zhong S.-Q., Li L., Dai Z.-G., 2023, ApJ, 947, L21
Zhu S.-Y., Sun W.-P., Ma D.-L., Zhang F.-W., 2024, MNRAS, 532, 1434
Zrake J., MacFadyen A. I., 2013, ApJ, 769, L29

This paper has been typeset from a TEX/LATEX file prepared by the author.